Available online at www.sciencedirect.com
SCIENCE DIRECT®
Journal of Sound and Vibration 290 (2006) 101–132
JOURNAL OF SOUND AND VIBRATION
www.elsevier.com/locate/jsvi

A wave model of a circular tyre. Part 1: belt modelling

R.J. Pinnington*

Institute of Sound and Vibration Research, University of Southampton, Southampton SO17 1BJ, UK

Received 7 January 2004; received in revised form 11 February 2005; accepted 16 March 2005
Available online 14 July 2005

Abstract

The equations of motion of a curved tyre belt are derived for one-dimensional waves propagating around the belt and a standing wave across the belt. The effects of curvature, shear stiffness, rotary inertia, tension, rotational speed and air pressure are included. These are combined to give a sixth-order wave equation, the solution of which gives three pairs of wavenumber as a function of frequency. The application of the boundary conditions at the contact leads to the input and transfer mobilities for both in-plane and out of plane excitation. Observed are: low-frequency rigid-body modes, belt bending modes and in-plane ring modes. At high frequencies only travelling waves occur.

1. Introduction

When a rotating tyre interacts with the road surface, as seen in Fig. 1, the time varying deformations are transmitted causing noise interior and exterior to the vehicle. To calculate this interaction with the road and also to determine the resulting vibration of the tyre surface it is first necessary to make a dynamic model of the tyre. Various tyre models have been developed for use in different frequency regimes. Finite element models [1] and the lumped parameter 'ring model' [2] are used for low-frequency vehicle handling and ride comfort, generally below 50 Hz. Vehicle interior noise is greatest between 50 and 500 Hz and the flexural modes of the belt that contribute have been modelled using both finite elements [1] and modal solutions to a wave equation [3–5].

*Corresponding author. Platia Skra 13, Kalamaria 55132, Thessaloniki, Greece. Tel./fax: +30 2310 480 645.
E-mail address: rjpinnington@compuserve.com.

0022-460X/$ - see front matter © 2005 Elsevier Ltd. All rights reserved.
doi:10.1016/j.jsv.2005.03.023

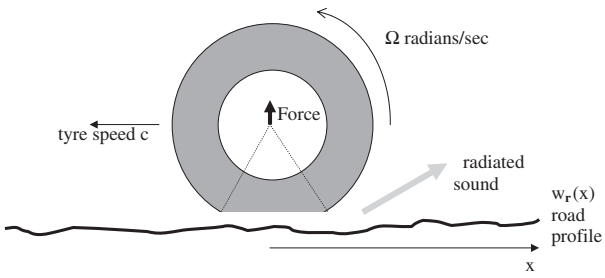

Fig. 1. Rotating tyre on a road profile.

The main exterior noise occurs between 500 and 3000 Hz, a region where there is little modal behaviour of the belt flexural waves. A flat orthotropic plate [4], and a deep flat two-layered plate [5], have been used with modal and travelling wave solutions. Also an infinite flat belt model that included tension, transverse shear, rotary inertia and bending was made for this region [6,7]. The dynamic behaviour was described by a fourth-order wave equation and input and transfer mobilities were obtained for transverse excitation. Below about 1 kHz, only tension and bending control the single propagating transverse wave; above this frequency a transverse shear wave and an in-plane rotational wave propagate.

The objective here is to extend this wave model to include: curvature, side-walls, asymmetric belt and tyre rotation to the other parameters, and thus make a complete circular belt model. A circular beam in Refs. [8,9], without the complications of side-wall, tension and cross modes has been investigated previously, for an energy flow application.

The main effect of curvature is to couple radial and circumferential motion thereby including the effects of both normal and tangential forces in all vibration responses of the tyre. A single model will therefore be made to embrace the whole frequency range of interest, from zero to 3 kHz, for both normal and tangential excitation. One-dimensional waves are allowed to propagate around the belt with a standing wave pattern in the transverse direction. The side-wall is modelled here from the static, pressure dependent, stiffness values taken from Ref. [7], a frequency-dependent side-wall is considered in the companion paper [10]. The waves in the air cavity are also neglected here, as they are only noticed at the first cavity resonance. They are, however, also included in Ref. [10], but not with full structural–acoustic coupling.

Tyre rotation has three effects that are included here. Firstly, waves in the direction of rotation have a corresponding speed increase, while waves in the opposite direction are slowed by the same amount. Secondly, the increase in belt tension to resist centrifugal forces. Finally, radial velocity couples with the rotation to cause Coriolis forces.

The equations of motion are combined to give a sixth-order wave equation for the circumferential waves of a particular transverse mode order m. There are three pairs of roots corresponding to the three waves that exist simultaneously at each frequency. The wavenumbers of these waves are plotted against frequency in the 'dispersion curves'. The ratio between radial and circumferential motion for each of these waves is also generated.

The boundary conditions at what would be the contact with the road are applied, giving the input and transfer mobilities for both radial and circumferential excitation. The transfer functions show: low-frequency rigid-body modes, mid-frequency tension/bending modes, and the in-plane mode group, beginning with the ring frequency around 500 Hz.

For line excitation only the waves of the $m = 0$ transverse order are included to give the transfer function. For point excitation the transfer functions from all the transverse mode orders are summed.

The results from the belt model developed here are compared with measurements in the companion paper [10].

2. Basic equations of motion

The overall scheme is shown in Fig. 1, where a tyre rotates in a positive or anti-clockwise sense at velocity V and angular velocity Ω. In the first instance it is assumed all the excitation arises from a transverse line of contact. To calculate the response to these forces the equations of motion for the tyre must be found.

Fig. 2a shows a segment of length δc and width δz, in a tyre belt of radius a and width b, displaying the sign convention for positive directions, rotations, forces and moments. It is assumed that the belt rotates about the offset wire reinforced neutral axis seen in Fig. 2b. It is also assumed that the averaged material properties of the cross-section are known, as reference will only be made to these single material values for the cross-section. Using the wave approach it is simple to make these material properties dependent on frequency, if required; but it is not necessary to state this dependency until the programming stage.

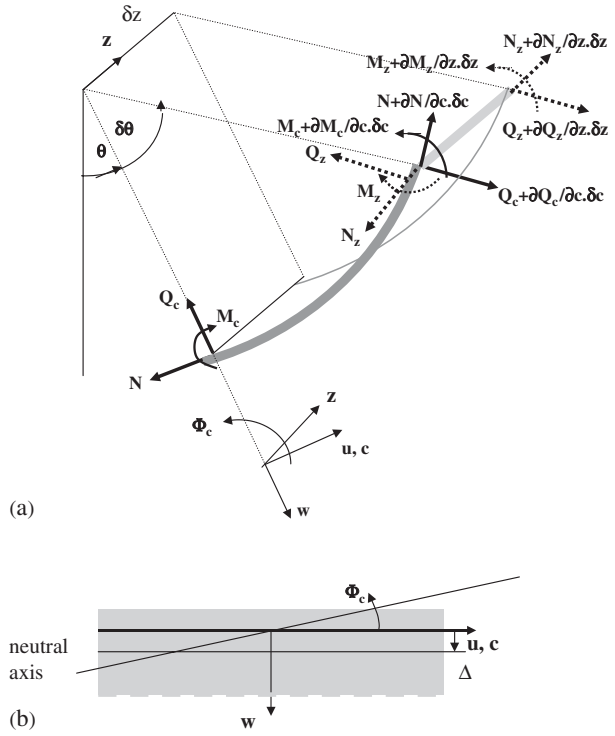

Fig. 2. (a) Sign convention for belt element and (b) asymmetric belt element.

The tyre could be described as a curved, tensioned, Mindlin plate on distributed two-directional stiffness. The belt is subjected to a net static pressure P which causes a static tension/length N_c, N_z in the circumferential and transverse directions c, z. Q_c, Q_z are the shear forces/length. N is the total static and dynamic circumferential force/width. M_c, M_z are the bending moments/length. The accompanying displacements are u, w, in the circumferential and radial directions. θ describes the geometric position and is related to the circumferential coordinate c by $a\theta$. The tyre rotates in the positive θ direction with velocity V. The belt is restrained either side by a side-wall of stiffness/belt length of K_c, K_r, in the circumferential and radial directions.

In this section three groups of equations are presented; kinematic relationships, equilibrium of forces and moments, and the linking Hooke's Law relationships.

2.1. Kinematic relationships

The segment motion can be described by three variables; displacements u, w and the kinematic rotation Φ. For a Mindlin plate that can deform in both bending and shear, the slope at any position s in the s and z directions are, respectively,

$$\frac{\partial w}{\partial c} = \beta_c + \gamma_c, \tag{1a}$$

$$\frac{\partial w}{\partial z} = \beta_z + \gamma_z, \tag{1b}$$

where β_c, β_z and γ_c, γ_z are the slopes due to bending and shear, respectively. The kinematic rotation, in the c direction, of the element Φ_c, seen in Figs. 2a and b, including that due to the circumferential displacement u, is therefore

$$\Phi_c = \frac{u}{a} - \frac{\partial w}{\partial c}. \tag{2a}$$

There is no geometric curvature in the z direction and so the rotation is simply

$$\Phi_z = -\frac{\partial w}{\partial z}. \tag{2b}$$

The total angle φ in the c direction is the sum of the geometric rotation θ and the kinematic rotation Φ_c. The small change in slope over the length δc is therefore

$$\delta\varphi = \left(\frac{1}{a} + \frac{\partial \Phi_c}{\partial c}\right)\delta c. \tag{3}$$

The circumferential strain ε_c also has contributions from both displacements

$$\varepsilon_c = \frac{\partial u}{\partial c} + \frac{w}{a}. \tag{4a}$$

The transverse strain ε_z only has a contribution from the transverse displacement u_z

$$\varepsilon_z = \frac{\partial u_z}{\partial z}, \tag{4b}$$

however, the transverse strain is ignored here and accordingly set to zero.

2.2. Force equilibrium equations

There are four equations of equilibrium: forces in the radial direction, forces in the circumferential direction (c), and for moments in the s and transverse (z) directions. The equilibrium of radial forces are taken in line with the circumferential shear force/width Q_c. Substitution of the segment rotation in Eq. (2a) yields the equation for equilibrium. For convenience, it is separated here into the equations for static and dynamic equilibrium. Eq. (5a) for static equilibrium is also calculated in Appendix A:

$$P + \mu\Omega^2 a - \frac{2N_z \sin\phi_1}{b} - \frac{N_c}{a} = 0,$$

$$p(c,z) + \frac{\partial Q_c}{\partial c} + \frac{\partial Q_z}{\partial z} - N_{cd}\left(\frac{1}{a} + \frac{\partial \Phi_c}{\partial c}\right) - N_c \frac{\partial \Phi_c}{\partial c} + N_z \frac{\partial^2 w}{\partial z^2} = \mu\ddot{w} - \left(\frac{P}{a} + \mu\Omega^2\right) w. \tag{5a,b}$$

P is the net static air pressure. $p(c,z)$ is the dynamic pressure due to the side-wall and external radial force, it is calculated in Section 2.24. N_z is the static transverse tensile force/length; N_c and N_{cd} are, respectively, the static and dynamic circumferential tensile forces/width; Q_z is the shear force/width in the radial direction. μ is the belt mass/area.

By resolving forces in the c direction in line with the circumferential force/width N, in Fig. 2a, and substitution of the segment rotation in Eq. (2a), gives

$$\tau(c,z) + \frac{\partial N}{\partial c} + \frac{\partial Q_{zc}}{\partial z} + Q_c\left(\frac{1}{a} + \frac{\partial \Phi_c}{\partial c}\right) = \mu(\ddot{u} + \Delta\ddot{\Phi}_c) + 2\mu\dot{w}\frac{(c+\dot{u})}{a} + \frac{2K_c}{b}u, \tag{6}$$

where K_c is the circumferential stiffness/belt length of a single side-wall. The tangential external stress is τ. Q_{zc} is the shear force/length in the circumferential direction. The wire reinforced neutral axis displaces u, however, the asymmetry of the belt about the neutral axis gives an inertial centroid which is displaced Δ, seen in Fig. 2b. The inertial centroid therefore accelerates by an additional rotation included in Eq. (6). The second term from the right is the Coriolis force, which gives gyroscopic coupling between the circumferential and radial motion. The nonlinear product of the radial and axial velocities is ignored in the later analysis.

The net moment, taken about the right-hand end z-axis of the segment is responsible only for the angular acceleration due to bending $\ddot{\beta}_c$ (as the shear component of slope is a distortion that does not involve overall rotation). The external moment/width M_0 that arises from the offset h from the neutral axis of the external shear force τ is also included

$$\frac{\partial M_0}{\partial c} = \tau h. \tag{7a}$$

Moment equilibrium about the z-axis yields

$$Q_c - \frac{\partial M_c}{\partial c} = I_c\ddot{\beta}_c + \frac{\partial M_0(s,z)}{\partial c}, \tag{7b}$$

where I_c is the belt moment of inertia/width. Similarly, the net moment about the right-hand side c-axis yields

$$Q_z - \frac{\partial M_z}{\partial z} = I_z \ddot{\beta}_z, \tag{7c}$$

where I_z is the belt moment of inertia/length about the c-axis.

2.3. Hooke's Law relationships

The three types of forces in Section 2.2 are assumed to be linearly related to the three deformation types given in Section 2.1. The constants of proportionality are the various elastic moduli of the belt section.

2.3.1. Circumferential stress–strain

The circumferential force/width N has a static component N_c and a dynamic component $N_{cd} = A_c \varepsilon_c$ arising from the circumferential strain

$$N = N_c + N_{cd}, \tag{8a}$$

where A_c is the belt circumferential stiffness/width. The tension N_c, calculated in Appendix A, Fig. 15, has two components, one determined from the pressure and tyre geometry, the other from resisting the datum centrifugal force $\mu\Omega^2 a$

$$N_c = Pa\left(1 - \frac{l_s}{b}\frac{\sin\phi_1}{\phi_s}\right) + \mu\Omega^2 a^2,$$

where l_s is the side-wall profile length and $2\phi_s$ is the angle subtended by the side-wall profile. The side-wall attaches to the belt at an angle ϕ_1. The static force/length in the transverse direction is also given in Appendix A

$$N_z = \frac{1}{2}\frac{Pl_s}{\phi_s}. \tag{8b}$$

2.3.2. Shear stress–strain relationships

In the circumferential direction the shear force/width Q_c is related to the shear strain γ_c by the belt shear stiffness/width S_c:

$$Q_c = S_c \gamma_c. \tag{9a}$$

Likewise in the transverse direction the shear force/width Q_z is related to the shear strain γ_z, by the belt shear stiffness/length S_z:

$$Q_z = S_z \gamma_z. \tag{9b}$$

The shear force in the circumferential direction normal to the z-axis Q_{zc} is controlled by the shear stiffness S_{zc}:

$$Q_{zc} = S_{zc}\frac{\partial u}{\partial z}. \tag{9c}$$

2.3.3. Bending moment–curvature

For a slender pre-curved beam of initial radius a the bending moment M_c is related to the total radius of curvature r and the bending stiffness/width B_c [11]:

$$M_c = B_c\left(\frac{1}{r} - \frac{1}{a}\right). \tag{10}$$

Ref. [12] gives the radius of curvature r as a function of the strain and kinematic rotation as

$$\frac{1}{r} = \left(\frac{1}{a} + \frac{\partial \Phi_c}{\partial c}\right)(1 - \varepsilon_c). \tag{11}$$

Therefore combining Eqs. (10) and (11) with a large initial curvature assumption, gives the bending moment-to-curvature relationship as

$$M_c = -B_c\left(\frac{\partial \Phi_c}{\partial c} - \frac{\varepsilon_c}{a}\right). \tag{12}$$

Making substitutions from Eqs. (1a), (2a) and (4a) the bending moment in the circumferential direction can now be written as

$$M_c = -B_c\left(\frac{\partial \beta_c}{\partial c} + \frac{w}{a^2}\right). \tag{13a}$$

The first term in the brackets is the curvature for a flat plate. The second term is the moment due to stretching of the neutral axis, becoming zero for a flat plate as the radius a tends to infinity. This is a simpler and slightly different expression for this relationship than is given in Ref. [8]. Likewise substitutions from Eqs. (1b), (2b) and (4b) give the bending moment in the transverse direction as

$$M_z = -B_z\left(\frac{\partial \beta_z}{\partial z}\right). \tag{13b}$$

This corresponds to the plane bending expression for a flat plate, where B_z is the bending stiffness in the transverse direction.

2.4. The ratio of shear rotation to bending rotation

For the circumferential direction, Eq. (1a) shows that the slope or rotation has two components γ_c, β_c, from shear and bending. The relative sizes of the bending slope to the total slope can now be found by eliminating unwanted variables from Eqs. (1a), (7b) and (13a) using a harmonic time dependency $e^{i\omega t}$, where ω and t are frequency in radians/second, and time.

$$\frac{\partial w}{\partial c}\left(\frac{B_c}{a^2} + S_c\right) = -B_c\frac{\partial^2 \beta_c}{\partial c^2} + (S_c - \omega^2 I_c)\beta_c. \tag{14a}$$

The corresponding version for the shear slope in the circumferential direction is found by substitution of Eq. (1a). Likewise in the transverse direction, the ratio of total slope to bending

slope is given from Eqs. (1b), (3b), and (13b)

$$\frac{\partial w}{\partial z}(S_z) = -B_z \frac{\partial^2 \beta_z}{\partial z^2} + (S_z - \omega^2 I_z)\beta_z. \tag{14b}$$

2.5. Equivalent modal stiffness

Eq. (5b) for radial equilibrium contains two terms with differentials in z and also a dynamic pressure term $p(c, z)$, associated with the side-wall stiffness. These three terms describing the belt transverse properties are all expressed as dynamic stiffness for the mth transverse mode of the belt. This procedure reduces Eq. (5) and the subsequent analysis to one-dimensional form, with only a c variation for each belt transverse mode order m.

2.5.1. Modal stiffness from the shear force and tension

If a harmonic wave solution of the form $\beta_z = \beta_z \exp(\mp i k_z z)$ is applied to Eq. (14b) the bending rotation can be written as

$$\beta_z = \left(\frac{S_z}{B_z k_z^2 + S_z - \omega^2 I_z} \right) \frac{\partial w}{\partial z}. \tag{15}$$

Substitution of this equation into Eqs. (1b) and (9b) gives the shear force in the transverse direction in terms of w:

$$Q_z = S_z \frac{B_z k_z^2 - \omega^2 I_z}{B_z k_z^2 + S_z - \omega^2 I_z} \frac{\partial w}{\partial z}. \tag{16}$$

This shear force term and the tension term N_z in Eq. (5) can now be written as a modal stiffness if some mode shapes can be selected to describe the radial motion in the z direction. To simplify this procedure it is assumed here that the belt construction is much heavier than that of the side-wall, which provides some justification for choosing boundary conditions at $z = \pm b/2$ that are; unconstrained in the radial direction but with zero slope. Also as the purpose here is not to accurately predict resonance frequencies but rather to demonstrate the physical behaviour, the simplest form, namely sine and cosine mode shapes are selected to satisfy these boundary conditions. These occur for a discrete set of wavenumbers $k_z = m\pi/b$, $m = 0, 1, 2, 3 \ldots$, i.e.

$$w(c, z) = \sum_{m=0,2,4\ldots} w_m(c) \cos \frac{m\pi z}{b} + \sum_{m=1,3,5\ldots} w_m(c) \sin \frac{m\pi z}{b}. \tag{17}$$

Using Eqs. (16) and (17) the two z-dependant terms in Eq. (5) can now be replaced by a modal stiffness K_{mz}, i.e.

$$\frac{\partial Q_z}{\partial z} + N_z \frac{\partial^2 w}{\partial z^2} = K_{mz} w, \tag{18}$$

where

$$K_{mz} = \left(\frac{m\pi}{b}\right)^2 \left(N_z + S_z \frac{B_z (m\pi/b)^2 - \omega^2 I_z}{B_z (m\pi/b)^2 + S_z - \omega^2 I_z} \right).$$

For the beam modes of the belt, denoted $m = 0$, there is no curvature in the z direction and so this modal stiffness is zero. For higher-order modes the stiffness increases with the square of the transverse belt mode order m, which determines the mode cut-on frequency. Above the cut-on frequency the mode forms in Eq. (17) propagate in the direction c.

2.5.2. The modal stiffness from the side-wall

The pressure on the belt $p(c,z)$ has two components, the external load p_0 and the pressure p_s from the side-wall displacement w at $z = \pm b/2$. These give rise to a pressure distribution on the belt

$$p(c,z) = -K_r[\delta(z-b/2)+\delta(z+b/2)]w(c,z) + p_0(c,z) \tag{19}$$

which may be expressed as a sum of modal pressures P_m:

$$p(c,z) = \sum_{m=0,2,4\ldots} P_m(c)\cos\frac{m\pi z}{b} + \sum_{m=1,3,5\ldots} P_m(c)\sin\frac{m\pi z}{b}. \tag{20}$$

Substitution of Eq. (17) into Eq. (19), and application of the orthogonality relations to Eqs. (19) and (20) allows the modal pressure terms to be written using the external modal pressure P_{0m} and a modal stiffness K_{rm}

$$P_m = -K_{rm}w_m + P_{0m}, \tag{21}$$

where for $m = 0$, $K_{rm} = 2K_r/b$; for $m>0$ $K_{rm} = 4K_r/b$.

All the terms in z found in Eq. (5) can now be replaced with the modal stiffness terms of Eqs. (18) and (21). The analysis now proceeds considering only wave motion in the c direction.

3. Equations of equilibrium in kinematic parameters

The three groups of equations of the previous sections can be combined to give the two equations of equilibrium of force only in terms of the displacements u, w.

3.1. Equation of radial equilibrium

The equation of radial equilibrium is found with three preliminary steps. These are to find the shear gradient, bending gradient, and the associated shear force. Eq. (5) of radial equilibrium is first expanded using Eqs. (1a), (2a), (4a), (7b), (8a), (9a), (12), (18) and (21), giving the gradients of the shear stress or shear strain.

The radial displacement for all subsequent analysis becomes w_m as each equation refers only to the displacement for the mth transverse mode, as expressed in Eq. (17), the other kinematic and force variables likewise have the modal subscript m, i.e. u_m, γ_m, β_m:

$$S_c\frac{\partial\gamma_m}{\partial c} = -P_{0m} + \frac{\partial u_m}{a\partial c}(N_c + A_c) - N_c\frac{\partial^2 w_m}{\partial c^2} + (A_c + (K_{zm}+K_{rm})a^2 - Pa - (\omega^2+\Omega^2)\mu a^2)\frac{w_m}{a^2}. \tag{22}$$

The gradient of the slope due to bending is the derivative of Eq. (1a)

$$\frac{\partial \beta_m}{\partial c} = \frac{\partial^2 w_m}{\partial c^2} - \frac{\partial \gamma_m}{\partial c}. \tag{23}$$

The shear force/width can be written, in the first instance, by expanding Eq. (7b) with Eq. (13a)

$$Q_m = -B_c\left(\frac{\partial^2 \beta_m}{\partial c^2} + \frac{\partial w_m}{a^2 \partial c}\right) - \omega^2 I_c \beta_m + \frac{\partial M_{0m}}{\partial c}. \tag{24}$$

By substituting Eq. (22) into Eq. (24), the shear force becomes

$$\begin{aligned} Q_m = & -\frac{B_c}{a^2 S_c}\left\{\begin{array}{l} a^2 \dfrac{\partial^3 w_m}{\partial c^3}(S_c + N_c) - \dfrac{\partial w_m}{\partial c}(A_c - S_c - Pa + (K_{zm} + K_{rm})a^2 - (\omega^2 + \Omega^2)\mu a^2) \\ -a \dfrac{\partial^2 u_m}{\partial c^2}(N_c + A_c) - a^2 \dfrac{\partial P_{0m}}{\partial c} \end{array}\right\} \\ & - \omega^2 I_c \beta_m + \frac{\partial M_{0m}}{\partial c}. \end{aligned} \tag{25}$$

This expression for shear force can now be differentiated with respect to c, then combined with Eq. (23) to eliminate $\partial\beta_m/\partial c$. The resulting expression for $\partial\gamma_m/\partial c$ is then substituted into Eq. (22), giving the equation for vertical equilibrium only in terms of u_m and w_m. It is presented here in a non-dimensional form which will be employed later in the wave equation

$$\begin{aligned} 0 = & -a^3 \frac{\partial^4 w_m}{\partial c^4}(\bar{S}_c + \bar{N}_c) + a \frac{\partial^2 w_m}{\partial c^2}\{C_1 - \bar{S}_c(1 + z_c^2) - \bar{N}_c C_2\} + \frac{w_m}{a} C_1 C_2 \\ & + (1 + \bar{N}_c)\left\{a^2 \frac{\partial^3 u_m}{\partial c^3} + \frac{\partial u_m}{\partial c} C_2\right\} + C_2 C_3 + f_m. \end{aligned} \tag{26}$$

In Eq. (26) some parameters have been grouped together in brackets ( ) as they share some physical significance

$$C_1 = 1 + \bar{K}_m - \bar{P}a - z_{Lc}^2 - Z_{ce},$$

$$C_2 = z_c^2 - \bar{R}_c,$$

$$C_3 = -\bar{P}_{0m},$$

$$f_m = a^2 \frac{\partial^2 \bar{P}_{0m}}{\partial c^2} + h\bar{R}_s \frac{\partial \bar{\tau}}{\partial c}, \tag{27a–c}$$

where

$$\bar{S}_c = \frac{S_c}{A_c}, \quad \bar{N}_c = \frac{N_c}{A_c}, \quad \bar{P}a = \frac{Pa}{A_c}, \quad \bar{R}_c = a^2 \frac{S_c}{B_c}, \quad \bar{K}_m = a^2 \frac{K_{rm} + K_{zm}}{A_c}, \quad Z_{ce} = a^2 \frac{\mu\Omega^2}{A_c}.$$

The external loading term f_m uses Eq. (7a) to write the moment M_{0m} in terms of shear stress τ. The normalised external pressures and shear stresses are defined as

$$\bar{P}_{0m} = a\,\frac{P_{0m}}{A_c}, \quad \bar{\tau}_m = a\,\frac{\tau_m}{A_c}.$$

The normalised non-dimensional circumferential wavenumber z_{Lc} is defined by

$$z_{Lc}^2 = (a\omega)^2\,\frac{\mu}{A_c}.$$

There is a wave that cuts on at high frequencies that involves only belt rotation and no translation, here it is called the 'rotational wave' [6], it could also be called the first asymmetric Lamb wave [13]. The wavenumber z_c is defined by

$$z_c^2 = (a\omega)^2\,\frac{I_c}{B_c}.$$

When $C_1 = 0$ the ring frequency occurs for the $m = 0$ waves, it increases with the side-wall radial stiffness K_r, but decreases with inflation pressure P and rotation speed. An instability occurs when the tyre speed drives the ring frequency to zero as the radial stiffness becomes zero.

When $C_2 = 0$ the rotational wave cuts on. This cut-on frequency increases with the section shear stiffness (proportional to belt depth), but decreases with the section moment of inertia (proportional to the cube of belt depth). The cut-on frequency is therefore inversely proportional to belt thickness.

For an infinite cylinder with no side-wall, static equilibrium gives $C_3 = 0$. For a finite width tyre it can be assumed that this term is negative, as the side-wall will take some of the tension.

The external load f_m has two components, the first is the radial load and the second is a moment from the tangential force.

For a flat belt with zero: tension, shear stiffness, side-wall stiffness, Eq. (26) reverts to the Euler beam bending equation.

3.2. The equation of circumferential equilibrium

Eq. (6) for circumferential equilibrium can be expanded with Eqs. (1a), (8a) and (9a) to yield

$$\bar{\tau}_m + a\,\frac{\partial^2 u_m}{\partial c^2} + \frac{\partial w_m}{\partial c}(1 - z_{Lc}^2\bar{\Delta}) + \bar{S}_c\gamma_m\left(1 + a\,\frac{\partial \Phi_m}{\partial c}\right) = \frac{u_m}{a}(\bar{K}_{cm} + \bar{K}_{zcm} - z_{Lc}^2) + \frac{w_m}{a}\,Z_{\mathrm{co}}, \qquad (28)$$

where the normalised radial side-wall stiffness derived in Eq. (21) is $k_z = m\pi/b$. The normalised cross mode shear stiffness is found from Eqs. (6) and (9c) by setting

$$\bar{K}_{cm} = 2a^2\,\frac{K_c}{A_c b} \text{ for } m = 0, \quad \bar{K}_{cm} = 4a^2\,\frac{K_c}{A_c b} \text{ for } m > 0, \quad \bar{K}_{zcm} = S_{zc}\left(\frac{m\pi}{b}\right)^2\frac{a^2}{A_c}.$$

The Coriolis term and centroid offset are

$$Z_{\mathrm{co}} = \frac{2\mathrm{i}\omega\mu c}{A_c}, \quad \bar{\Delta} = \frac{\Delta}{a}.$$

This equation will now be simplified using the following justification. The non-dimensional shear stiffness $\bar{S}_c$, defined in Eq. (26), is the ratio of the average section shear stiffness to circumferential stiffness. For a tyre belt the shear stiffness is dominated by the rubber, and the circumferential stiffness by the embedded steel wires; the shear stiffness ratio is likely to be of the order of 0.01, allowing this final term on the left hand to be ignored in the proceeding analysis.

For a homogeneous material it is also probably safe to ignore this term for three reasons. First the second term in the bracket forms a nonlinear product $\gamma_m \partial\phi_m/\partial c$, which is also very small. The greatest value of the shear ratio for a homogeneous material e.g. for steel, $\bar{S}_c \approx 0.3$, and as from Eq. (1) $\gamma \leqslant \partial w/\partial c$, the greatest possible error in the shear wavenumber from the omission is 30%. The equation for circumferential equilibrium can therefore be written in the reduced form below

$$\bar{\tau}_m + a\frac{\partial^2 u_m}{\partial c^2} + \frac{\partial w_m}{\partial c}(1 - z_{Lc}^2\bar{\Delta}) = \frac{u_m}{a}(\bar{K}_{cm} + \bar{K}_{zcm} - z_{Lc}^2) + \frac{w_m}{a}Z_{\mathrm{co}}. \tag{29}$$

For a flat beam $a \to \infty$ and Eq. (29) becomes that for longitudinal motion of a rod. The cross-coupling to radial motion w is purely geometric, and increases with decreasing radius a. The term in brackets, C

$$C_4 = \bar{K}_{cm} + \bar{K}_{zcm} - z_{Lc}^2 \tag{30}$$

becomes zero at the rotational rigid-body resonance of the belt ($n = 0$). At this frequency the belt rotates on the side-wall shear stiffness. At $1/\sqrt{2}$ of this frequency the $n = 1$ translation rigid-body resonance occurs. Below these frequencies there is mainly rigid-body motion of the belt.

3.3. The wave equation for a circular tyre belt

The wave equation for a free belt is given by combining Eqs. (26) and (29), but setting the load terms f_m and τ_m to zero. A harmonic solution for a wave travelling in the positive c direction, of the form $\mathrm{e}^{-\mathrm{i}kc}$, is applied. Then by substituting for w_m using Eq. (29), the sixth-order wave equation is obtained in the normalized wavenumber $z_m = k_m a$

$$\begin{aligned}
0 = {} & z_m^6(\bar{S}_c + \bar{N}_c) \\
& - z_m^4[z_{Lc}^2(1 - \bar{\Delta}(1 + \bar{N}_c)) + \bar{P}a + Z_{ce} - \bar{K}_m - \bar{N}_c\bar{R}_c + (\bar{S}_c + \bar{N}_c)(1 + z_c^2 + z_{Lc}^2 - \bar{K}_{cm} - \bar{K}_{zcm})] \\
& + z_m^2\begin{bmatrix}(\bar{K}_{cm} - \bar{K}_{zcm} - z_{Lc}^2)(1 + \bar{K}_m - \bar{P}a - \bar{S}_c - z_{Lc}^2 + Z_{ce} + \bar{N}_c\bar{R}_c - z_c^2(\bar{S}_c + \bar{N}_c)) \\ + (z_c^2 - \bar{R}_c)(\bar{N}_c - \bar{K}_m + \bar{P}a + Z_{ce} + z_{Lc}^2(1 - \bar{\Delta}(1 + \bar{N}_c)))\end{bmatrix} \\
& + (1 + \bar{K}_m - \bar{P}a - Z_{ce} - z_{Lc}^2)(z_c^2 - \bar{R}_c)(z_{Lc}^2 - \bar{K}_{cm} - \bar{K}_{zcm}) \\
& \pm \mathrm{i}(1 + \bar{N}_c)(z_m^3 - (z_c^2 - \bar{R}_c)z_m)Z_{\mathrm{co}}.
\end{aligned} \tag{31}$$

The components within the brackets are functions of frequency or constants. The material properties can be complex to include hysteretic damping; they can also be written as functions of frequency (as is the case for polymers).

The final term with the odd wavenumber orders is the Coriolis coupling, the $\pm$ is for the anti-clockwise and clockwise waves, respectively. This term may be significant in the contact patch but not for a circular tyre, and so is ignored in this initial study.

The equation in z_m^2 is solved at each frequency to give three pairs of roots $p = 1, 2, 3$ for each transverse mode group m. The normalised wavenumbers are of the form z_{pm} i.e. $\pm z_{1m}, \pm z_{2m}, \pm z_{3m}$, '+' denotes the positive or anti-clockwise travelling wave, '−' denotes the negative or clockwise travelling wave. The subscript m will be omitted in the following discussion for the sake of simplicity.

In this analysis the three selected wavenumbers k_p will take the sign and form of the wave that exists in the positive direction. The corresponding wave in the negative direction is always assumed to take the opposite sign. The roots are complex in general, and all the possibilities are plotted in Fig. 4. The true roots or waves are those that *decay in the anti-clockwise direction* and have the possibilities $(\pm k_r - \mathrm{i}k_i)$, where k_r and k_i are the real and imaginary wavenumbers. These roots are those of the lower half of the figure. The correct anti-clockwise wave therefore takes the form

$$\exp(-\mathrm{i}k_p c) = \exp(\mp \mathrm{i}k_r c)\exp(-k_i c).$$

This wave can be of three types

1. $k_r \gg k_i$, a propagating or travelling wave, seen just below the real axis. For zero damping this root lies on the axis, damping causes this root and all the others to rotate in a clockwise direction.
2. $k_i \gg k_r$, the evanescent bending wave is purely imaginary for zero damping, the damping gives small negative real part.
3. $k_r \approx k_i$ is termed the 'complex wave', which always occurs in a pair $\pm k_r - \mathrm{i}k_i$ (labelled 1, 2) to form a rapidly decaying standing wave, which usually describes a local stiffness characteristic.

3.4. Wavenumbers modified by tyre rotation

All the displacements are functions of wavenumber, defined in the frame of reference of the tyre. However, in practice the tyre is rotating in relation to the axle, and wavenumbers are perceived from this reference to differ from those of the reference frame of the tyre. This is true only for travelling waves, where energy is stored within the tyre as both kinetic and strain energy. However, the situation is less clear for the evanescent and complex 'waves' which exist only to satisfy the boundary conditions in the locality of the excitation. The complex wave describes stiffness and will therefore not be affected by the rotation, which acts on inertia. Alternatively, it could be said that the phase speed for a complex wave is infinite and so will not be significantly perturbed by rotation. The evanescent bending wave represents inertia and so is expected to be influenced by rotation, but this effect is ignored here because of the difficulty in isolating the root in the program. The changes for the travelling waves only were made as follows.

The wave phase speeds for anti-clockwise and clockwise travelling waves are the same, i.e. V_p, $p = 1, 2, 3$ for no rotation. If the tyre rotates anti-clockwise at velocity V, the travelling waves change velocity relative to the wheel axle and line of contact (but the waves still travel at their original velocities in relation to the belt). The modified wave speeds relative to the axle are

$$\begin{aligned} V_{pa} &= V_p + V, \\ V_{pb} &= V_p - V. \end{aligned} \tag{32}$$

The anti-clockwise wave becomes V_{pa}, faster by V; while the clockwise wave V_{pb} slows by V. Using the relationship, $k_p = \omega V_p$, the wavenumbers become

$$k_{pa} = \frac{k_p}{1 + \mathrm{Re}\{k_p\} V/\omega}, \quad k_{pb} = \frac{k_p}{1 - \mathrm{Re}\{k_p\} V/\omega}. \tag{33}$$

Note that both wavenumbers are positive here, the appropriate negative sign for the negative travelling wave is included in the analysis of the next section.

Only the real part of wavenumber is related to energy transfer and is employed in the denominator. If there is no rotation: $k_b = k_p$, $k_{pa} = k_p$.

4. Belt transfer functions

Fig. 3 shows the tyre belt subjected to external forces at the contact point $\theta = 0$. *All the forces, moments, kinematic quantities, and wavenumbers in the following analysis are assumed to refer to a particular belt lateral mode of order m, until the final discussion on the transfer functions.*

If a normal force F_y or a tangential force F_x is applied to the tyre it causes responses at every point c, in both the circumferential u and radial w directions. These responses are quantified in the transfer functions. All the transfer functions can be calculated from the summation of the three pairs of waves that exist at each frequency. The amplitudes of these waves are found from the six boundary conditions at the contact line with the force input, corresponding to the road contact with the tyre.

A matrix of radial wave amplitudes is written. These are used to give: slopes ϕ, in-plane displacements, shear rotation α, bending rotation β, in-plane forces N, shear forces Q and moments M. The six boundary conditions are then expressed as a matrix in terms of the radial displacements. The solution of this matrix gives the wave amplitudes and hence the transfer functions.

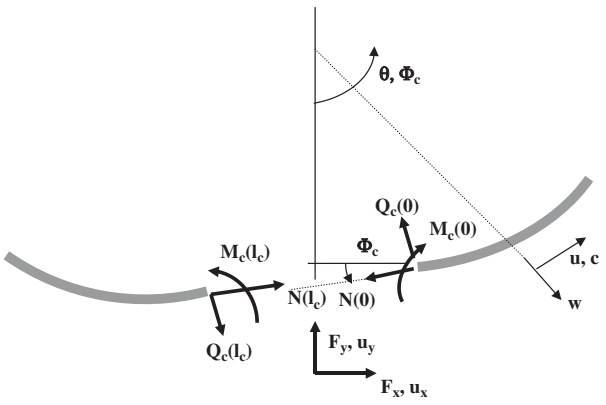

Fig. 3. Forces on the belt at the contact line.

4.1. The wave field

The radial displacement w, and circumferential displacement u, at any point c are written as a sum of the three wave pairs. The gradient of each wave also has two components due to bending and shear, respectively.

4.1.1. Radial displacement

The wavenumbers for the three wave pairs obtained from the wave equation are: k_{pa}, k_{pb}, $p = 1, 2, 3$; a (anti-clockwise), b (clockwise), denote the direction of the wave propagation. If there is no rotation, $k_{pa} = k_{pb} = k_p$ for all waves. From Eq. (33), rotation only causes a change to the travelling wave, i.e. $0 < k_{pa} < k_p < k_{pb}$.

The radial amplitudes of each of the three pairs of waves: w_{pa}, w_{pb}, are given in a column matrix $\mathbf{w}_p$.

$$\mathbf{w}_p = \begin{Bmatrix} w_{1a} \\ w_{1b} \\ w_{2a} \\ w_{2b} \\ w_{3a} \\ w_{3b} \end{Bmatrix}. \tag{34}$$

At position c each wave becomes phase-lagged and attenuated in accordance with the 6×6 diagonal matrix $\mathbf{L}_{pc}$:

$$\mathbf{L}_{pc} = \mathrm{diag}[\mathrm{e}^{-\mathrm{i}k_{1a}c}, \alpha_{1b}\mathrm{e}^{\mathrm{i}k_{1b}c}, \mathrm{e}^{-\mathrm{i}k_{2a}c}, \alpha_{2b}\mathrm{e}^{\mathrm{i}k_{2b}c}, \mathrm{e}^{-\mathrm{i}k_{3a}c}, \alpha_{3b}\mathrm{e}^{\mathrm{i}k_{3b}c}], \tag{35}$$

where the exponential attenuation and phase-lag over the belt circumference $l_c = 2\pi a$ is

$$\alpha_{pa} = \exp(-\mathrm{i}k_{pa}l_c), \quad \alpha_{pc} = \exp(-\mathrm{i}k_{pb}l_c).$$

The column matrix for weighted wave amplitude and phase is $\mathbf{w}_{pc}$:

$$\mathbf{w}_{pc} = \mathbf{L}_{pc}\mathbf{w}_p. \tag{36}$$

The radial displacement $w(c)$ at any point c is the sum of the six waves in Eq. (36)

$$w(c) = \mathbf{I}^{\mathrm{T}}\mathbf{w}_{pc}, \tag{37}$$

where the row matrix $\mathbf{I}^{\mathrm{T}} = \{1\ 1\ 1\ 1\ 1\ 1\}$ is just a device to make the sum.

The slope at any point c is obtained using the differential operator $\mathbf{D}_p$:

$$\frac{\partial w}{\partial c} = \mathbf{I}^{\mathrm{T}}\mathbf{D}_p\mathbf{w}_{pc}, \tag{38}$$

where $\mathbf{D}_p = \mathrm{diag}[-\mathrm{i}k_{1a}, \mathrm{i}k_{1b}, -\mathrm{i}k_{2a}, \mathrm{i}k_{2b}, -\mathrm{i}k_{3a}, \mathrm{i}k_{3b}]$.

4.1.2. Circumferential displacement

The circumferential displacement u_{pa} is the radial displacement w_{pa} weighted by the displacement ratios A_{pa} and A_{pb} for anti-clockwise and clockwise pth wave.

$$u_{pa} = A_{pa}w_{pa}, \quad u_{pb} = A_{pb}w_{pb}. \tag{39a,b}$$

The displacement ratios for the anti-clockwise and clockwise waves are found by substituting the harmonic travelling wave solutions $\exp(\mp \mathrm{i}k_p c)$ into Eq. (29)

$$A_{pa}, A_{pb} = \frac{\mp \mathrm{i} z_{pa}(1 - z_L^2 \bar{A}) - Z_{\mathrm{co}}}{z_{pa}^2 - z_L^2 + \bar{K}_{cm} + \bar{K}_{zcm}}. \tag{40a,b}$$

The Coriolis coupling Z_{co} is set to zero in this study. The total circumferential displacement $u(c)$ is the sum of the six wave displacements $\mathbf{u}_p$ in Eq. (36)

$$u(c) = \mathbf{I}^{\mathrm{T}} \mathbf{A}_p \mathbf{w}_{pc}. \tag{41}$$

The diagonal matrix of displacement ratios is

$$\mathbf{A}_p = \mathrm{diag}[A_{1a}, A_{1b}, A_{2a}, A_{2b}, A_{3a}, A_{3b}].$$

4.1.3. The slope due to bending

The gradient $\partial w/\partial c$ is given in Eq. (1a) as the sum of the bending slope β and the shear γ. Slope due to bending is related to the gradient by Eq. (14a). On substitution of the harmonic solution for a clockwise or anti-clockwise travelling wave p, and using the normalisation of Eq. (26)

$$\boldsymbol{\beta}_p = \mathbf{E}_p \frac{\partial \mathbf{w}_p}{\partial c}, \tag{42}$$

where

$$E_{pa} = E_{pb} = \frac{1 + \bar{R}_c}{z_p^2 - z_c^2 + \bar{R}_c}.$$

The diagonal matrix of wave weighting functions E_{pa}, E_{pb} is

$$\mathbf{E}_p = \mathrm{diag}[E_{1a}, E_{1b}, E_{2a}, E_{2b}, E_{3a}, E_{3b}]. \tag{43}$$

4.2. The boundary conditions

There are six boundary conditions all at the contact line. Three are geometric continuity relations linking the belt either side of the contact line. The other three are the resolution of the two external forces and moment, into the internal forces. All the boundary conditions are expressed in terms of the six radial wave amplitudes $\mathbf{w}_p$.

4.2.1. Continuity of radial displacement

There is continuity in the radial displacement at $\theta = 0$, $\theta = 2\pi$, or $c = 0$, $c = l_c$, where l_c is the belt length. From Eqs. (36) and (37)

$$0 = \mathbf{B}_{1p} \mathbf{w}_p, \tag{44}$$

where

$$\mathbf{B}_{1p} = \mathbf{I}^{\mathrm{T}}(\mathbf{L}_{pc}(0) - \mathbf{L}_{pc}(l_c))$$

or

$$\mathbf{B}_{1p} = [1 - \alpha_{1a} \quad \alpha_{1b} - 1 \quad 1 - \alpha_{2a} \quad \alpha_{2b} - 1 \quad 1 - \alpha_{3a} \quad \alpha_{3b} - 1].$$

4.2.2. Continuity of circumferential displacement

There is continuity of circumferential displacement at $c = 0$, $c = l_c$, so equating these displacements using Eqs. (36) and (41) gives

$$0 = \mathbf{B}_{2p}\mathbf{w}_p, \tag{45}$$

where

$$\mathbf{B}_{2p} = \mathbf{I}^{\mathrm{T}}\mathbf{A}_p(\mathbf{L}_{pc}(0) - \mathbf{L}_{pc}(l_c))$$

or

$$\mathbf{B}_{2p} = [A_{1a}(1 - \alpha_{1a}) \quad A_{1b}(\alpha_{1b} - 1) \quad A_{2a}(1 - \alpha_{2a}) \quad A_{2b}(\alpha_{2b} - 1) \quad A_{3a}(1 - \alpha_{3a}) \quad A_{3b}(\alpha_{3b} - 1)].$$

4.2.3. Continuity of slope due to bending

Slope due to bending β, is continuous across the input line. However slope due to the shear γ, is discontinuous because of the external shear force. Continuity of slope due to bending can be expressed as $\beta(0) = \beta(l_c)$, or using Eqs. (36), (38), (42) and (43)

$$0 = \mathbf{B}_{3p}\mathbf{w}_p, \tag{46}$$

where

$$\mathbf{B}_{3p} = \mathbf{I}^{\mathrm{T}}\mathbf{E}_p\mathbf{D}_p(\mathbf{L}_{pc}(0) - \mathbf{L}_{pc}(l_c)).$$

This can be expanded to give the 6×1 row matrix

$$\mathbf{B}_{3p} = [-\mathrm{i}k_{pa}E_{pa}(1 - \alpha_{pa}) \quad \mathrm{i}k_{pb}E_{pb}(\alpha_{pb} - 1).....], \quad p = 1, 2, 3.$$

4.2.4. Bending moment

An external moment will be applied in any practical situation because the external in-plane force is applied at the tread surface rather than at the neutral axis. The external moment M_0 is balanced by the internal moments at $c = 0$ and l_c, i.e.

$$M_0 = M_c(l_c) - M_c(0).$$

If substitution is made from Eq. (13a)

$$M_0 = B_c\left[\frac{\partial\beta_c}{\partial c} - \frac{w}{a}\right]_{c=0} - B_c\left[\frac{\partial\beta_c}{\partial c} - \frac{w}{a}\right]_{c=l_c}. \tag{47}$$

By differentiating Eq. (42) with respect to c, and using the continuity in w, this becomes

$$M_0 = \mathbf{B}_{4p}\mathbf{w}_p, \tag{48}$$

where

$$\mathbf{B}_{4p} = B_c \mathbf{I}^{\mathrm{T}} \mathbf{E}_p \mathbf{D}_p^2 (\mathbf{L}_{pc}(0) - \mathbf{L}_{pc}(l_c)).$$

Expansion of this expression gives a 6×1 row matrix

$$\mathbf{B}_{4p} = B_c[-k_{pa}^2 E_{pa}(1-\alpha_{pa}) \quad -k_{pb}^2 E_{pb}(\alpha_{pb}-1).....], \quad p = 1,2,3.$$

4.2.5. Normal force resolution

The normal force/width F_y, seen in Fig. 3, can be resolved into the component internal shear forces/width Q_c, and circumferential forces/width N, at $c = 0,\ c = l_c$

$$F_y = [Q_c - N\Phi_c]_{c=0} - [Q_c - N\Phi_c]_{c=l_c}, \tag{49}$$

where the kinematic rotation Φ_c, is given in Eq. (2a). The circumferential force/width N is given from Eq. (8a) as the dynamic force and N_c, the static in-plane force/width. The shear force for the pth wave can be expanded using Eqs. (1a), (9a) and (43). $\mathbf{I}_0$ is the unit matrix

$$\mathbf{Q}_p = S_c(\mathbf{I}_0 - \mathbf{E}_p)\frac{\partial \mathbf{w}_p}{\partial c}. \tag{50}$$

If only the static circumferential force is considered, i.e. $N = N_c$, then substitution into Eq. (49) of Eqs. (2a), (38), (41), (43) and (50), yield

$$F_y = \mathbf{B}_{5p}\mathbf{w}_p, \tag{51}$$

where

$$\mathbf{B}_{5p} = \mathbf{I}^{\mathrm{T}}\left((S_c + N_c)\mathbf{D}_p - S_c\mathbf{E}_p\mathbf{D}_p - \frac{N_c}{a}\mathbf{A}_p\right)(\mathbf{L}_{pc}(0) - \mathbf{L}_{pc}(l_c)).$$

On expanding the terms this becomes the following 6×1 row matrix:

$$\mathbf{B}_{5p} = [B_{51a} \quad B_{51b}\vdots \quad B_{52a} \quad B_{52b}\vdots \quad B_{53a} \quad B_{53b}].$$

For the pth pair of anti-clockwise and clockwise coefficients $B5_{pa}B5_{pb}$

$$[B5_{pa} \quad B5_{pb}] = \begin{bmatrix} \left\{ \mathrm{i}k_{pa}(S_c(1-E_{pa}) + N_c) - \dfrac{N_c}{a}A_{pa} \right\}(\alpha_{pa}-1) \\ \left\{ \mathrm{i}k_{pb}(S_c(1-E_{pb}) + N_c) - \dfrac{N_c}{a}A_{pb} \right\}(\alpha_{pb}-1) \end{bmatrix}, \quad p = 1,2,3.$$

4.2.6. Tangential force resolution

Resolution of the tangential forces seen in Fig. 3 yields

$$F_x = N(l_c) - N(0), \tag{52}$$

where F_x is the external tangential force/width, N is the circumferential force/width defined in Eq. (8a). By making substitutions from Eqs. (8a) and (4a), the tangential force becomes

$$F_x = A_c\left(\frac{\partial u}{\partial c}+\frac{w}{a}\right)_{c=l_c} - A_c\left(\frac{\partial u}{\partial c}+\frac{w}{a}\right)_{c=0} \tag{53}$$

which is, on using the amplitude ratio of Eq. (41) with Eqs. (36) and (38)

$$F_x = \mathbf{B}_{6p}\mathbf{w}_p, \tag{54}$$

where

$$\mathbf{B}_{6p} = -A_c\mathbf{I}^{\mathrm{T}}\left(\mathbf{D}_p\mathbf{A}_p+\frac{1}{a}\mathbf{I}_0\right)(\mathbf{L}_{pc}(0)-\mathbf{L}_{pc}(l_c)).$$

Eq. (54) may be further expanded as a row matrix of three pairs

$$\mathbf{B}_{6p} = [B_{61a} \quad B_{61b}\vdots B_{62a} \quad B_{62b}\vdots B_{63a} \quad B_{63b}].$$

The pth pair is

$$[B_{6pa} \quad B_{6pb}] = \left[A_c(\alpha_{pa}-1)\left(-\mathrm{i}k_{pa}A_{pa}+\frac{1}{a}\right) \quad A_c(1-\alpha_{pb})\left(\mathrm{i}k_{pb}A_{pb}+\frac{1}{a}\right)\right], \quad p=1,2,3.$$

4.3. The belt transfer functions

The six boundary conditions may now be assembled into a single matrix. The solution of this matrix gives the required transfer functions for either normal or tangential excitation. The boundary conditions that sum to zero are found in Eqs. (44)–(46), (50), those with an external force are in Eqs. (51), (54). The boundary conditions are written as a stiffness matrix $\mathbf{K}$

$$\mathbf{F} = \mathbf{K}\mathbf{w}_p, \tag{55}$$

where the force matrix $\mathbf{F}$ includes the two external forces, $\mathbf{w}_p$ are the wave radial displacement amplitudes

$$\mathbf{F} = \begin{Bmatrix} 0 \\ 0 \\ 0 \\ M_0 \\ F_y \\ F_x \end{Bmatrix}, \quad \mathbf{K} = \begin{bmatrix} \mathbf{B}_{1p} \\ \mathbf{B}_{2p} \\ \mathbf{B}_{3p} \\ \mathbf{B}_{4p} \\ \mathbf{B}_{5p} \\ \mathbf{B}_{6p} \end{bmatrix}, \quad \mathbf{w}_p = \begin{Bmatrix} w_{1a} \\ w_{1b} \\ w_{2a} \\ w_{2b} \\ w_{3a} \\ w_{3b} \end{Bmatrix}.$$

Inversion of Eq. (55) gives the radial wave amplitudes

$$\mathbf{w}_p = \mathbf{K}^{-1}\mathbf{F}. \tag{56}$$

The circumferential wave amplitudes weight these by the amplitude ratio in Eq. (41)

$$\mathbf{u}_p = \mathbf{A}_p \mathbf{w}_p. \tag{57}$$

The displacements $w(c)$, $u(c)$ at any point c are found by multiplying the wave amplitudes with the position weighting 6×1 row matrix from Eqs. (36) and (37)

$$\mathbf{I}^{\mathrm{T}}\mathbf{L}_{pc} = \{\exp(-\mathrm{i}k_{pa}c) \quad \alpha_{pb}\exp(\mathrm{i}k_{pb}c).....\}, \quad p = 1,2,3,$$

$$w(c) = \mathbf{I}^{\mathrm{T}}\mathbf{L}_{pc}\mathbf{w}_p, \quad u(c) = \mathbf{I}^{\mathrm{T}}\mathbf{L}_{pc}\mathbf{u}_p. \tag{58a,b}$$

4.3.1. Radial and circumferential mobility for a normal force

The radial and circumferential mobility for a normal force is obtained by modifying the force column matrix in Eq. (55); $\mathbf{F}_x = 0$, $\mathbf{M}_0 = 0$, $\mathbf{F}_y = -\mathbf{F}_{ym}$, where $\mathbf{F}_{ym}$ refers specifically to the force applied to the mth transverse belt mode. The negative sign arises because the applied force in Fig. 3 is in the negative radial direction. The responses in Eq. (58) are also replaced by the specified modal equivalent, i.e. $w_m(c) = w(c)$, $u_m(c) = u(c)$. Then Eqs. (56)–(58) give

$$\frac{\dot{w}_m(c)}{F_{ym}} = Y_m^{yy}(c) = \mathrm{i}\omega\mathbf{I}^{\mathrm{T}}\mathbf{L}_{pc}\mathbf{K}^{-1}\mathbf{F},$$

$$\frac{\dot{u}_m(c)}{F_{ym}} = Y_m^{xy}(c) = \mathrm{i}\omega\mathbf{A}_p\mathbf{K}^{-1}\mathbf{F}. \tag{59}$$

$Y_m^{yy}(c)$, $Y_m^{xy}(c)$, are the modal mobilities at position c in the radial and circumferential directions, respectively. The modal forces for any line force $F_{ym}(z)$ can be found from the modal decomposition equation:

$$F_y(z) = \sum_{m=0,2,4...} F_{ym}\cos\frac{m\pi z}{b} + \sum_{m=1,3,5...} F_{ym}\sin\frac{m\pi z}{b}. \tag{60}$$

For the particular case of a *point force* at z, i.e. $F_y(z) = F_0\delta(z - z_0)$ the orthogonality relations applied to Eq. (60), i.e.

$$\int_{z=-b/2}^{z=b/2} .....\left(\cos\frac{m\pi z}{b} + \sin\frac{m\pi z}{b}\right)\mathrm{d}z$$

yields

$$F_{y0} = \frac{F_0}{b}_{m=0}, \quad F_{ym} = \frac{2F_0}{b}\left(\cos\frac{m\pi z_0}{b}_{m=2,4...} + \sin\frac{m\pi z_0}{b}_{m=1,3...}\right). \tag{61}$$

The modal force from a *line force* of total magnitude F_0 applied over the belt width b is the first term in Eq. (61) i.e. $F_{y0} = F_0/b$.

The velocity response in the radial and circumferential directions, to a unit point radial force, is a sum of the modal contributions in Eq. (59), with the modal forces available

from Eq. (61):

$$Y^{yy} = \sum_{m=0,1,2,3....} Y_m^{yy},$$
$$Y^{xy} = \sum_{m=0,1,2,3...} Y_m^{xy}. \quad (62a, b)$$

4.3.2. Radial and circumferential mobilities for a circumferential force

The mobilities for a unit line circumferential force acting on the neutral axis are obtained by modifying the force column matrix in Eqs. (55), (59); $F_x = 1/b$, $F_y = 0$, $M_0 = 0$, where b is the belt width.

4.3.3. Radial and circumferential mobilities for a tangential force on the surface

The mobilities for a unit line circumferential force acting tangentially on the surface are obtained by modifying the force column matrix in Eqs. (55), (59); $F_x = 1/b$, $F_y = 0$, $M_0 = t/b$, where b is the belt width and t the distance from the surface to the neutral axis. The circumferential displacement on the surface $\mathbf{u}'_{ps}$ includes a component from the belt rotation from Eqs. (36)–(38)

$$\mathbf{u}'_{pc} = \mathbf{u}_{pc} + t\mathbf{D}_p\mathbf{w}_{pc}. \quad (63)$$

5. Parameter study

Some parameters seen in Table 1, were selected for the physical properties of a typical automobile tyre; they are a modified version of those used in Refs. [6,7]. Using these properties the

Table 1
Belt parameters

	Symbol		Size or equation		Units
Internal pressure	P		2×10^5		N/m^2
Belt thickness	t		1.6×10^{-2}		m
Belt radius	a		0.3		m
Belt width	b		0.16		m
Side-wall length	l_s		0.1		m
Side-wall angle	θ_s		$\pi/6$		rad
Tensile force/width	N_c	N_z	Eq. (A.4)	$P \times l_s/2\theta_s$	N/m
Shear moduli	G_c	G_z	5×10^7	5×10^7	N/m^2
Shear stiffness/width	S_c	S_z	$G_c \times t$	$G_z \times t$	N/m
Bending stiffness/width	B_c	B_z	107	90	Nm
Axial stiffness/width	A_c		1×10^7	∞	N/m
Belt mass/area	μ		16		kg/m^2
Rotational inertia/width	I_c	I_z	$\mu \times t^2/3$	$\mu \times t^2/3$	kg
Bending and shear loss factor	η_1	η_1	0.15	0.15	
Axial and tension loss factor	η_2	η_2	0.1	0.1	
Side-wall stiffness/length	K_r	K_c	1.4×10^6	2.1×10^5	N/m^2

following related quantities are generated and discussed for the $m = 0$ wavegroup generated by line excitation, namely, the wavenumbers, the ratio between radial and longitudinal motion, the slopes due to bending and shear, and radial and circumferential mobilities. Finally, a modal summation is made and the point and transfer mobilities are plotted.

5.1. Wavenumber as a function of frequency

For Figs. 5–7, a consistent notation is employed to identify the roots of the anticlockwise wavenumbers: — root 1, - - - - root 2, ... root 3. The properties of each root will be discussed with reference to these figures. The issues are: the significant frequency ranges, and the wave mechanism in each frequency range.

All the results are plotted between 10 Hz and 10 kHz, covering the practical range of interest. Fig. 5a shows the three wavenumber magnitudes, or wavenumber radii given in Fig. 4. Fig. 5b displays the corresponding phase Φ of each wavenumber, where $\Phi = \tan^{-1}(k_i/k_r)$. The phase of

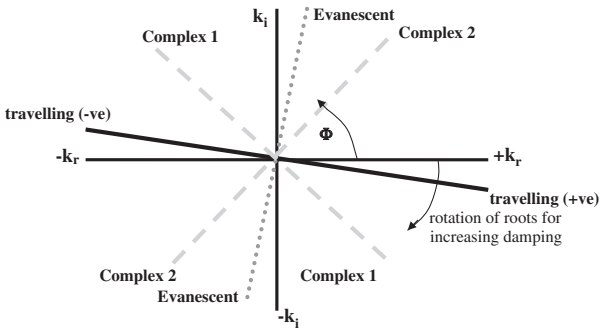

Fig. 4. Types of wavenumber roots.

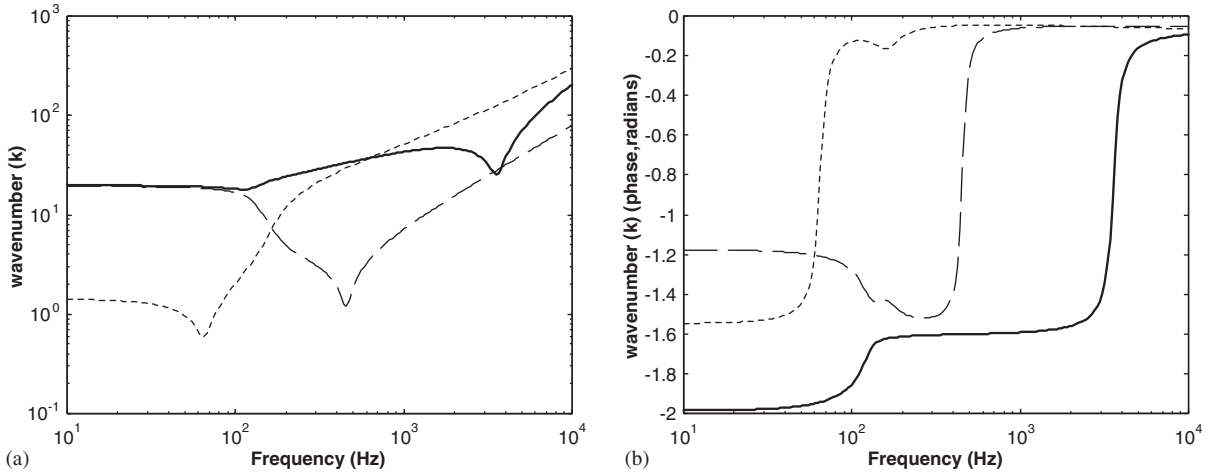

Fig. 5. (a) Modulus and (b) phase of wavenumbers: ▬ root 1, - · - · - · root 2, · · · · · · root 3.

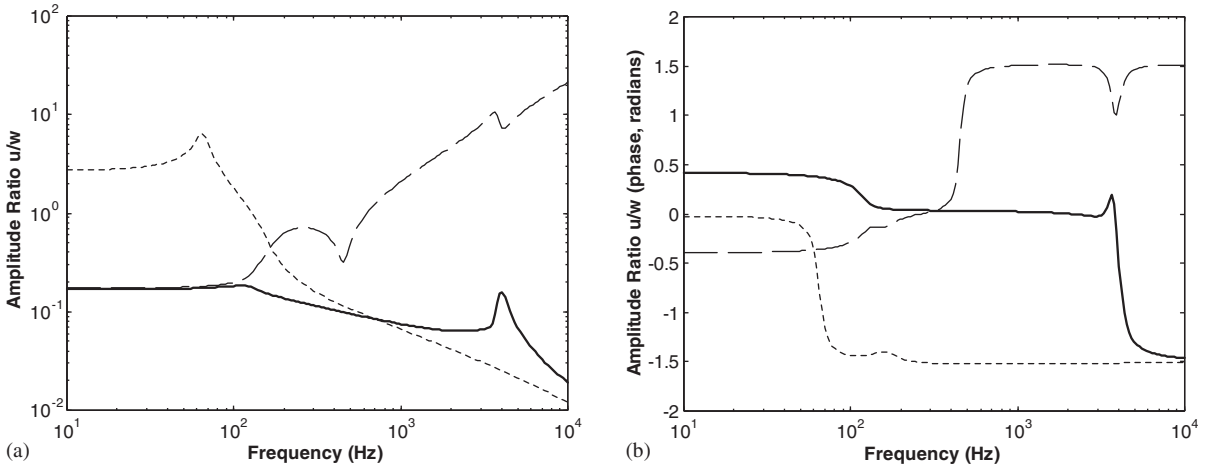

Fig. 6. (a) Modulus and (b) phase of amplitude ratio u/w: ▬ root 1, − · − · − root 2, ····· root 3.

all anti-clockwise wavenumbers lie between 0 and $-\pi$ as was indicated in Fig. 4. Figs. 6a and b give the modulus and phase of the ratio A_p of longitudinal motion to transverse motion for each root. Figs. 7a and b display, for each wave, the ratio of shear slope to bending slope.

5.1.1. *Wavenumber root 1*

Roots 1 and 2 seen in Fig. 5a are a complex pair of constant equal modulii below 120 Hz. The roots are symmetric about the negative imaginary axis in Fig. 4; or alternatively in Fig. 5b, the wavenumber phases are equally greater and less than the imaginary axis value of $-\pi/2$. In Fig. 6a it is shown that their dominant motion is radial rather than circumferential. In this frequency range, below the rigid body translational mode at 120 Hz, these two roots are responsible for the local stiffness controlled deformation around the contact line (Section 5.2.1).

Between 120 Hz and 3 kHz root 1 is an evanescent bending wave. This is evident from the modulus, in Fig. 5a, increasing as $(\text{frequency})^{1/2}$, while the phase is near $-\pi/2$. The phase is slightly more negative than this because of the material damping. Fig. 6a also indicates that the motion is predominately radial. At 3 kHz there is a dip in the wavenumber modulus and a large step in the phase in Fig. 6b, to almost 0 rad. This behaviour marks the cut-on of the rotational travelling wave, identifiable as a travelling wave from a wavenumber phase near zero. The form of this wave is suggested from Figs. 6 and 7. From Fig. 6 it is seen to be a radial wave. From Fig. 7a and b the bending and shear components are in anti-phase, but the shear part is just dominant. This implies that this wave does not have a large net radial component and may therefore be able to propagate in the tyre contact patch, where radial motion is not encouraged excitation.

The wave speed at high frequencies is close to that of the speed of sound, and so this could contribute to sound radiation, particularly for in-plane shear excitation in the contact region.

5.1.2. *Wavenumber root 2*

The second root forms the complex complement of root 1 until the rigid-body translational resonance at 120 Hz, as discussed above. Between 120 Hz and the ring-frequency at 450 Hz the phase of near $-\pi/2$ suggest no propagation. Above the ring-frequency the root cuts on and

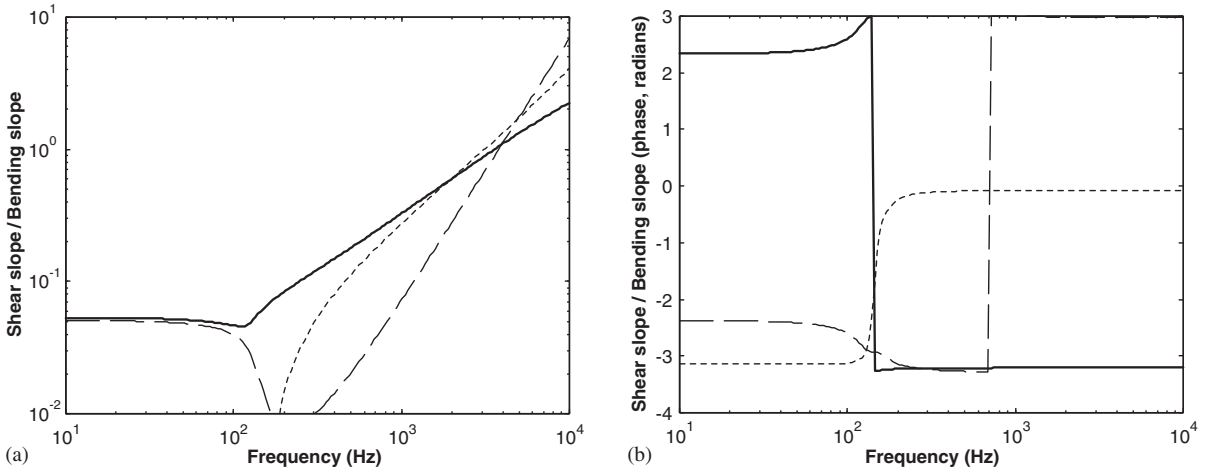

Fig. 7. (a) Modulus and (b) phase of shear slope/bending slope: ▬ root 1, – · – · – root 2, ····· root 3.

propagates as a longitudinal wave. This wave is identified from three things: the slope proportional to frequency (in Fig. 5a), a near zero phase (in Fig. 5b), and a dominant longitudinal motion in Fig. 6a. The wave speed is 800 m/s and is therefore able to radiate sound freely.

5.1.3. *Wavenumber root 3*

At 60 Hz the rigid-body rotation resonance occurs, of the belt mass upon the side-wall shear stiffness. Below this frequency root 3 is responsible for describing the rigid-body motion. The wavelength can be calculated, from the wavenumber in Fig. 5a, to be one tyre circumference as for the $n = 1$ mode.

At higher frequencies a propagating wave cuts on, seen from the near zero phase in Fig. 5a. Figs. 6a and 7a show it to be a bending wave below the rotational wave cut-on at 3 kHz. The wave only propagates above the frequency of the $n = 1$ mode at 120 Hz, when the belt resonates on the side-wall. Above this frequency the travelling wave is responsible for any discernible standing wave below the ring-frequency at 450 Hz. The wave is controlled by belt tension and bending stiffness, although the slope in Fig. 5a above 200 Hz is proportional to $(\text{frequency})^{1/2}$ suggesting the bending is dominant here.

The wave becomes shear dominated above 3 kHz as may be deduced from: the predominately radial motion in Fig. 6a, the greater shear motion in Fig. 7a. The wave speed is 200 m/s at 10 kHz which is less than the speed of sound in air. Radiation of sound is only expected from the discontinuity at the excitation line.

5.2. *Transfer functions for line excitation in the radial and circumferential directions*

The wavenumbers can now be used in the assembly of transfer functions using the procedures of Section 4. The force is normal or tangential and is applied at the contact line at 0°. The velocity response is calculated at the same position to give input mobility, it is also calculated at 180° to give the transfer mobility. Radial and longitudinal (circumferential) mobilities are given in Figs. 8 and 9. The tangential mobility at the tyre surface due to longitudinal

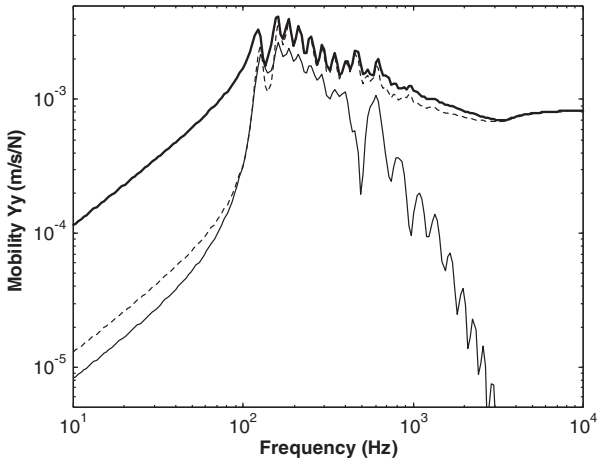

Fig. 8. Radial mobilities: — transfer modulus at 180°, ▬ input modulus, ····· input real part.

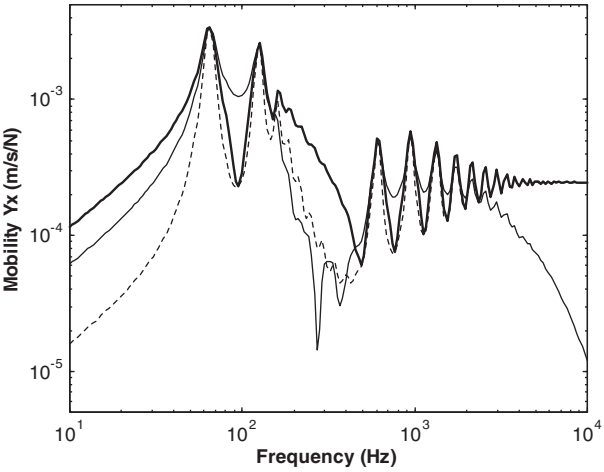

Fig. 9. Longitudinal mobilities: — transfer modulus at 180°, ▬ input modulus, ····· input real part.

and radial motion is given in Fig. 10. Finally, two parameter variations are presented in Figs. 11 and 12, showing the effects of pressure and tyre speed.

5.2.1. *Radial mobilities*

Fig. 8 gives radial mobilities at the input at 0°, and 180°, from a normal force at the contact line at 0°. The real part of the input mobility is always positive which implies that the model is physically possible. Below the rigid body transverse mode $n = 1$ at 120 Hz, the input mobility modulus is controlled by the local stiffness, generated from the complex roots 1 and 2. The transfer mobility is accordingly at least an order of magnitude lower. Between 120 and 450 Hz the $n = 1, 2, 3, \ldots$ bending wave resonance frequencies, from root 3, can be seen. The transfer mobility

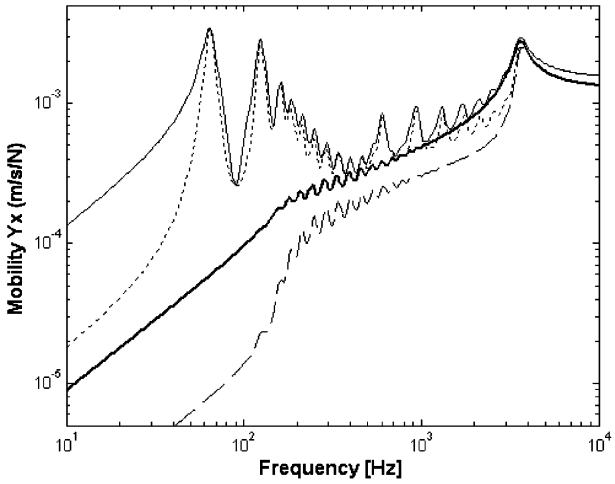

Fig. 10. Input tangential mobilities: ▬ moment modulus, ····· real part for moment, — total tangential modulus, – · – · – total tangential real part.

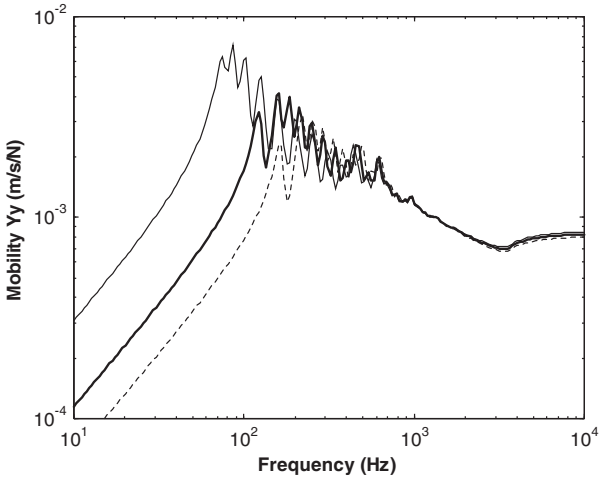

Fig. 11. Input radial mobility as a function of inflation pressure: — 0.5 bar, ▬ 2 bar, ····· 4 bar.

levels are lower because there is no contribution from the evanescent bending wave, and the waves are attenuated by the damping.

At 450 Hz the ring-frequency occurs, $n = 0$, when a longitudinal wavelength (root 2), fits around the circumference. A larger peak is seen at this frequency at the input; but a trough occurs in the transfer mobility. The ring mode is therefore only local to the excitation as suggested by the non-zero root 2 wavenumber phase, in Fig. 5b. This may explain why this phenomenon is not easily observed in measurements. The second longitudinal wave resonance is seen near 1 kHz on all plots.

The input modulus and real part of mobility have a slope of (frequency)$^{-1/2}$ until 3 kHz as for a beam in pure bending. At 3 kHz the rotation wave cuts on, but the main response above this

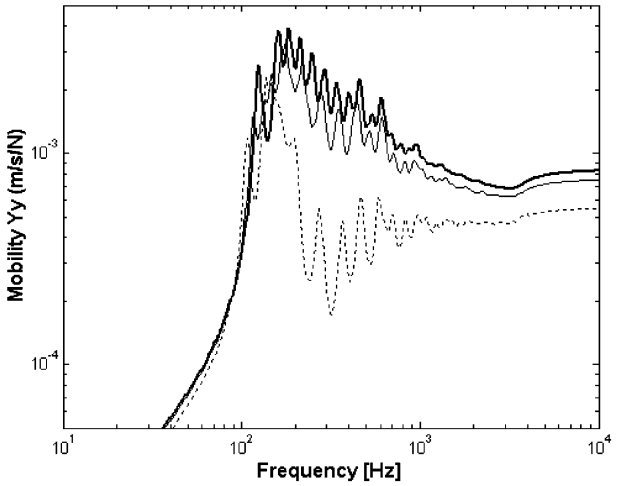

Fig. 12. Real part of input radial mobility as a function of speed: — 0 m/s, ▬ 40 m/s, ····· 80 m/s.

frequency is from the transverse shear wave, identified as root 3 in Fig. 5. For a different excitation, for example by a moment, the rotation wave may be larger. Above 1 kHz the transfer mobility reduces sharply as these waves have a short wavelength giving a high attenuation.

5.2.2. Longitudinal mobility on the neutral axis

Fig. 9 displays the real part and modulus of the input longitudinal mobility, and also the modulus of the transfer mobility at 180°. At 60 Hz the belt has a rigid body $n = 0$ rotational resonance. Below this frequency the tyre rotates and translates as a rigid body, as described by root 3 in Fig. 5; the side-wall shear stiffness controls the response level. At 120 Hz the belt rigid body translation resonance occurs, denoted as $n = 1$. Above this frequency the response level drops until a minimum at the ring frequency at 450 Hz. The coupling with transverse motion causes a slight excitation to the bending modes in this region. At 600 Hz the lowest excited longitudinal mode is seen, the remainder of the sequence is clearly visible until 3 kHz. In this region the transfer mobility is similar to the input mobility, which could mean that these waves are sufficiently large to make a detectable contribution to radiated sound levels. The mean input mobility takes the value of a longitudinally excited infinite rod.

5.2.3. Moment mobility and tangential mobility

In Section 4.3.3, it was shown that the tangential input mobility is the sum of the in-plane response seen in Fig. 9, and the response to the moment about the neutral axis. The real component and modulus of this moment component is displayed in Fig. 10. Also shown is the real part and modulus of the total input tangential mobility. Below about 1 kHz the tangential mobility is similar to the longitudinal mobility. However, near 3 kHz the cut on of the rotational wave causes a major peak in the response. This peak dominates the response due to the moment alone. It seems likely that this local resonance could contribute significantly in the tyre squeal phenomena as it is excited by tangential forces and moves primarily tangentially to the surface.

5.2.4. The effect of tyre pressure on transverse input mobility

Fig. 11 displays the transverse input mobility modulus as a function of tyre pressure. It is seen that the increase in pressure has two effects. The most significant is that it increases the radial sidewall stiffness thereby raising the frequency of the lowest radial natural frequency and decreasing the total response level. The second less noticeable effect is the resulting increase of tyre tension. This causes a stiffening of the belt below the ring frequency and so tends to raise natural frequencies and decrease the response in this region. These two effects are at low frequencies and would influence the vibration and noise within the vehicle.

5.2.5. The effect of tyre speed on the input transverse mobility

The tyre speed has two effects on the tyre vibration. The first is the change to the clockwise and anti-clockwise wavenumbers, which was discussed in Section 3.5. The second is the increasing centrifugal force on the belt which contributes to the tension, as described in Appendix A. These two influences are seen in Fig. 12 for the mobility modulus and real part. The overall response becomes lower from the belt stiffening and the decrease of the anti-clockwise wavenumbers. These two mechanisms also cause a decrease in wavenumber which leads to increase in sound radiation. Mode splitting is only noticeable on the first mode because of the high attenuation of the clockwise wave due to the increase in wavenumber. The range in the figure, 0–40 m/s, covers normal driving operation where the change in mobility due to speed is less than a factor of two.

When the rotational speed is equal to the phase speed due to tension, a shock wave will develop at the leading edge of the contact zone. A lot of power is absorbed by the tyre as the impedance becomes very large, making failure likely. The 80 m/s seen in the figure is near the limit for this particular tyre. If a puncture occurs in a tyre, the loss in pressure will cause a decrease in wavespeed giving the possibility of this failure mechanism at lower driving speeds. Tyres with a high pressure would be more vulnerable.

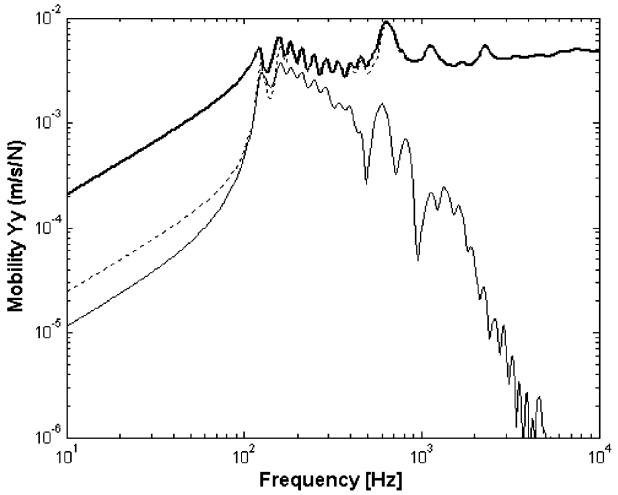

Fig. 13. Radial point mobility: ▬ input modulus, ····· input real part, — transfer modulus at 180°.

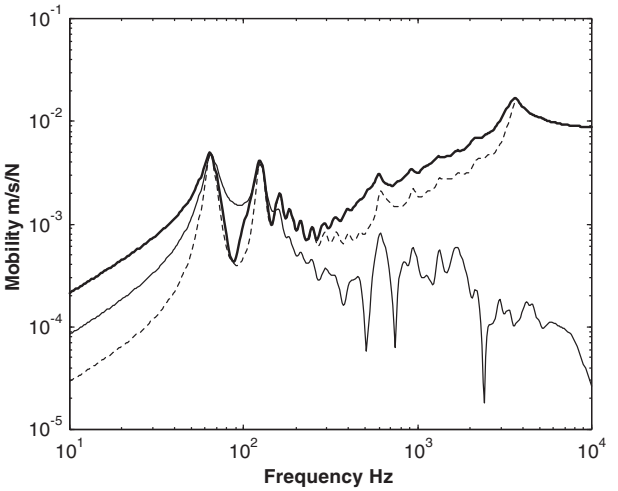

Fig. 14. Tangential point mobility: ▬ input modulus, ····· input real part, — transfer modulus at 180°.

5.2.6. *The effect of an offset neutral axis*

The effect of the non-alignment of the neutral axis and centroidal axis was investigated, but the changes were so small that it was considered that a plot was unnecessary.

5.3. *Tyre mobilities for point excitation*

If there is point excitation rather than line excitation, the higher order mode groups, $m>0$, are summed with the $m=0$ response in accordance with Eq. (62a). Figs. 13 and 14 show the modulus and real part of the input point mobility along with the transfer mobility at 180°. The excitation and response were displaced from the centre line by a distance $z_0 = b/10$.

Fig. 13 gives the input and transfer mobilities in the radial direction. Below 300 Hz the frequency structure is similar to the $m=0$ version in Fig. 8, except that the input response is greater on account of the presence of the stiffness component of the higher order modes. At about 0.6, 1.1, 1.7, 2.2 kHz humps in the input response indicate the cut-on of the $m=1,2,3,4,\ldots$ transverse mode groups. Only modes $m=0$–8 were included in the summation with the top cut-on frequency at about 4 kHz. This explains why the slope is less than proportional to frequency, as would be expected for a plate controlled by shear stiffness. Limiting the mode count in this way simulates the effect of an excitation diameter of $b/8$.

Fig. 14 shows the input and transfer mobilities in the circumferential direction for tangential excitation. The result is similar to that for $m=0$, in Fig. 10, except that the levels above 500 Hz are greater due to the summation of transverse modes. The four cut-on frequencies of the transverse modes $m=1,2,3,4$ are the same as for normal excitation, as the response is dominated by the radial wave motion excited by the input moment. The 'resonance' from the rotational wave cut on at 3 kHz is a clear feature, and is therefore expected to have an important role in the dynamics of tangential motion and high-frequency sound generation.

Similar high frequency, normal and tangential excitation results are seen in Ref. [4].

6. Conclusions

A sixth-order differential wave equation was derived to describe the motion of a curved tyre in the frequency range between 0 Hz and 4 kHz, for point or line excitation, in the radial and tangential directions. The model included the effects of: longitudinal stiffness, bending stiffness, shear stiffness, tension, pressure, speed, side-wall stiffness in two directions, mass and rotary inertia.

The solution of this equation is three pairs of waves at each frequency. These waves are described in terms of frequency dependency, ratio of circumferential to radial motion, ratio of shear slope to bending slope, and amplitude and phase. The waves are used to assemble radial and longitudinal transfer functions.

The behaviour of the tyre may be roughly divided into three frequency regions. First is the belt rigid body region that occurs below the rigid body translational resonance frequency. At this resonance the belt mass is mainly restrained by the side-wall radial stiffness. There is also local stiffness deformation at the contact. The belt mass, pressure and tyre geometry are main influences. If the pressure increases the rigid body frequency is raised and the tyre becomes stiffer, lowering the mobility.

The second frequency region lies between the rigid body resonance and the belt ring frequency, around 500 Hz. Standing waves are observed on the belt in the radial direction. The behaviour is controlled by belt tension and bending stiffness. The tension is a function of pressure and tyre rotational speed; increasing these increases the stiffness and raises the resonant frequencies. The belt moves as a rigid body in the longitudinal direction.

At about 500 Hz the belt ring frequency occurs. Above this frequency longitudinal waves can propagate within the belt and the coupling due to curvature between longitudinal to transverse motion decreases. The ring frequency mode seems to be a local resonance around the excitation line. The longitudinal waves propagate with relatively low attenuation and because of their long wavelengths may contribute to the sound radiation.

In the lateral direction waves become strongly attenuated and only travelling waves are observed, the belt behaves as if of infinite extent. Around 3 kHz a new wave cuts on which involves rotation without much transverse motion. At the same time the bending wave converts to a transverse shear wave, controlled by the belt shear stiffness. This wave dominates the radial motion.

The effect of tyre speed was investigated. The general trend is to reduce the mobility at all frequencies due to the combined influence of centrifugal force, and speed dependent wavenumber changes. This would increase the power absorbed and radiated by the tyre.

Acknowledgement

The support by the EC fifth framework program of the RATIN project is gratefully acknowledged.

Appendix A. Tyre belt and side-wall tension

A segment of length $2a\delta\theta$ and belt radius a, of a tyre cross-section is displayed in Fig. 15. The belt mass/area is μ. The transverse and circumferential belt tension/width N_z, N_c and the side-wall

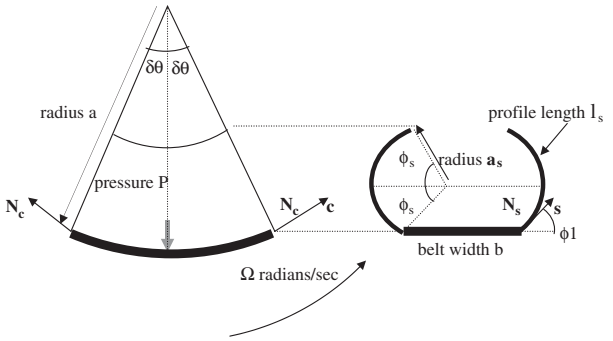

Fig. 15. Belt segment and cross-section.

elements, are only a function of the pressure and geometry. The belt tension/length N_c is found from the equations of equilibrium in the horizontal and radial directions. The tyre rotates at Ω rad/s giving a belt velocity c m/s. The side-wall is the arc of a circle of radius a_s subtending an angle $2\phi_s$. The arc is rotated making an angle ϕ_1 with the horizontal.

By considering the horizontal equilibrium of the right-hand side-wall element

$$N_z = P.a_s, \tag{A.1}$$

where the side-wall radius a_s is related to the side-wall arc length l_s by

$$a_s = \frac{l_s}{2\phi_s}. \tag{A.2}$$

The radial equilibrium of the belt segment can now be taken along the centre line

$$0 = ((P + \Omega^2\mu a)a.b - N_c b - 2N_z a \sin\phi_1)2\delta\theta. \tag{A.3}$$

This includes contributions from the pressure, centrifugal force, belt tension and side-wall tension, respectively. By making substitutions from Eqs. (A.1) and (A.2), Eq. (A.3) can be re-arranged to give the belt tension:

$$N_c = Pa\left(1 - \frac{l_s}{b}\frac{\sin\phi_1}{\phi_s}\right) + \Omega^2 a^2 \mu. \tag{A.4}$$

References

[1] H. Ishiara, Development of a three dimensional membrane element for the finite element analysis of tires, *Tire Science and Technology* 13 (2) (1985).
[2] P.W.A. Zegelaar, S. Gong, H.B. Pacejka, Tyre models for the study of in-plane dynamics, in: *The Dynamics of Vehicles on Roads and Tracks*, *Vehicle System Dynamics*, Swets & Zeitlinger, 1994.
[3] W. Kropp, Structure-sound on a smooth tyre, *Applied Acoustics* 20 (3) (1989) 181–193.
[4] K. Larsson, W. Kropp, A high frequency tyre model based on two coupled elastic layers, *Journal of Sound and Vibration* 253 (4) (2001) 889–908.
[5] S. Gong, A Study of In-plane Dynamics of Tires, PhD Thesis, Delft University of Technology, Faculty of Mechanical Engineering and Marine Technology, 1993.

[6] R.J. Pinnigton, A.R. Briscoe, A wave model for a pneumatic tyre belt, *Journal of Sound and Vibration* 253 (2002) 941–959.
[7] R.J. Pinnington, Radial force transmission to the hub from an unloaded stationary tyre, *Journal of Sound and Vibration* 253 (2002) 961–983.
[8] S.J. Walsh, R.G. White, Mobility of a semi-infinite curved beam with constant curvature, *Journal of Sound and Vibration* 221 (1999) 887–902.
[9] S.J. Walsh, R.G. White, Vibrational power transmission in curved beams, *Journal of Sound and Vibration* 223 (3) (2000) 455–488.
[10] R.J. Pinnington, A wave model for a circular tyre. Part 2: side-wall and force transmission modelling, *Journal of Sound and Vibration*; doi:10.1016/j.jsv.2005.03.024.
[11] P.P. Benham, F.W. Warnock, *Mechanics of Solids*, Pitman, New Zealand, Wellington, 1979.
[12] S. Timoshenko, *Theory of Elastic Stability*, McGraw-Hill, New York, 1936.
[13] L. Cremer, M.L. Heckl, E.E. Ungar, *Structure-borne Sound*, Springer, Berlin, 1973.